Cell

The First Five Seconds in the Life of a Clathrin-Coated Pit

Emanuele Cocucci,[1,2] François Aguet,[1] Steeve Boulant,[1,2,3] and Tom Kirchhausen[1,2,*]
[1]Department of Cell Biology, Harvard Medical School, Boston, MA 02115, USA
[2]Immune Disease Institute and Program in Cellular and Molecular Medicine at Boston Children's Hospital, Boston, MA 02115, USA
[3]Present address: Laboratory of Viral Infection and Innate Immune Sensing Dynamics, Ruprecht-Karls-Universität, Heidelberg 69117, Germany
*Correspondence: kirchhausen@crystal.harvard.edu
http://dx.doi.org/10.1016/j.cell.2012.05.047

SUMMARY

Coated pits assemble by growth of a clathrin lattice, which is linked by adaptors to the underlying membrane. How does this process start? We used live-cell TIRF imaging with single-molecule EGFP sensitivity and high temporal resolution to detect arrival of the clathrin triskelions and AP2 adaptors that initiate coat assembly. Unbiased object identification and trajectory tracking, together with a statistical model, yield the arrival times and numbers of individual proteins, as well as experimentally confirmed estimates of the extent of substitution of endogenous by expressed, fluorescently tagged proteins. Pits initiate by coordinated arrival of clathrin and AP2, which is usually detected as two sequential steps, each of one triskelion with two adaptors. PI-4,5-P_2 is essential for initiation. The accessory proteins FCHo1/2 are not; instead, they are required for sustained growth. This objective picture of coated pit initiation also shows that methods outlined here will be broadly useful for studies of dynamic assemblies in living cells.

INTRODUCTION

Membrane traffic establishes, maintains, and reorganizes most of the principal compartments of a cell. It does so while retaining the compositional and functional heterogeneity of the donor and acceptor membranes. Clathrin-coated vesicles, the first membrane traffic carriers recognized and analyzed in detail, have become a paradigm for efforts to understand molecular mechanisms of other modes of vesicular transport (Harrison and Kirchhausen, 2010). They carry cargo, such as transferrin, immunoglobulins, low-density lipoprotein (LDL), hormones, and signaling receptors, from the plasma membrane to endosomes and between endosomes and the trans-Golgi network.

The "canonical" coated pit is an invaginating structure in which assembly of a curved clathrin lattice, linked by adaptors and other proteins to deformation of the underlying membrane, gives rise to a coated vesicle by constriction and (dynamin-catalyzed) scission (Kirchhausen, 2009; Traub, 2009). Because it takes place at the cell surface, coated pit assembly is particularly favorable for detailed molecular analysis by live-cell fluorescence microscopy. Our current picture of the stages in the formation of coated pits and coated vesicles derives primarily from real-time imaging of living cells by total internal reflection fluorescence (TIRF) and spinning-disk confocal microscopy to follow the formation of coated pits and vesicles at the plasma membrane (Ehrlich et al., 2004; Gaidarov et al., 1999; Mettlen et al., 2010; Saffarian et al., 2009; Taylor et al., 2011). We can formally distinguish several sequential stages corresponding to nucleation, growth and invagination, budding and scission, and uncoating. The whole cycle occurs in about 1 min.

The most important structural components of the coat are clathrin and its AP2 (α-β2-μ2-σ2) heterotetrameric adaptor complex. Coated pit formation proceeds by sequential addition of clathrin triskelions and adaptors, generating a sharply curved coat; adaptor-mediated interactions with membrane-bound proteins (and lipids) deform the underlying membrane; dynamin mediates scission when the deformation has created a suitably narrow neck; and auxilin, which arrives immediately following scission, recruits Hsc70 to direct uncoating (Lee et al., 2006; Massol et al., 2006). Hip1R, which binds clathrin light chains, recruits actin, which is required in some instances for coated-vesicle maturation and budding (Ferguson et al., 2009; Gottfried et al., 2009; Merrifield et al., 2002; Saffarian et al., 2009). A number of accessory proteins associate with coated pits at specific stages of assembly and disassembly (Henne et al., 2010; Reider et al., 2009; Toshima et al., 2006; Traub, 2009), but their functions are less certain. Eps15, epsin, FCHo1 and FCHo2 (FCHo1/2), and intersectin form a complex that appears to collect at the rim of a coated pit (Henne et al., 2010; Reider et al., 2009; Saffarian et al., 2009; Tebar et al., 1996). This "rim complex" accumulates during early stages of coated pit assembly, but its components are excluded from a budded coated vesicle. It has been proposed that the rim complex components are required for coated pit initiation because coated vesicles fail to form in their absence. Other, nonessential components are required for incorporation of particular cargo molecules (Goodman et al., 1996; Miller et al., 2011; Yu et al., 2007).

Our present understanding of coated pit initiation comes from ensemble biochemical assays and from live-cell imaging that did not achieve levels of sensitivity and temporal resolution required

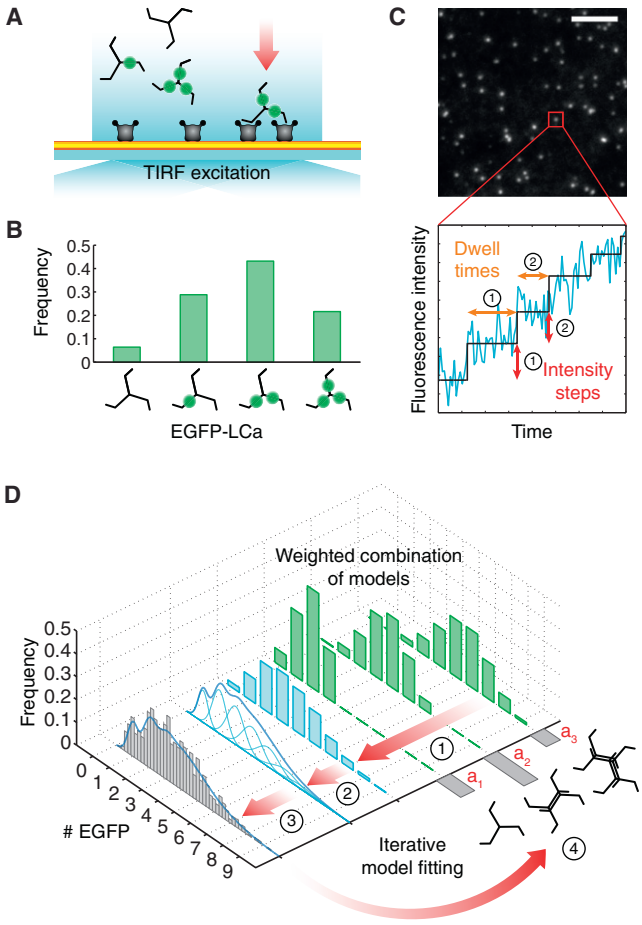

Figure 1. Schematic Representation of the Experimental Setup and Computational Analysis

(A) TIRF imaging setup used for the experiments. This illustration shows an example of the recruitment of clathrin and AP2 adaptors to the plasma membrane (yellow) of a cell attached through the modified PEG support to a glass coverslip. Each clathrin triskelion contains three light chains that, depending on the expression level, might or might not be replaced by ectopically expressed EGFP-LCa (green). The imaging experiments used here were designed to detect and track with single-molecule sensitivity the arrival of the first clathrin (or AP2) molecules to the site of coated pit initiation.

(B) Distribution of numbers of triskelions containing none, one, two, or three EGFP-LCa molecules. Incorporation of EGFP-LCa follows a binomial distribution, as shown in this example for a replacement of 60%.

(C) Frame from a TIRF time series showing fluorescent spots corresponding to coated pits labeled with clathrin EGFP-LCa. Scale bar, 5 μm. The fluorescence intensity trace (blue) corresponds to the profile from a single clathrin-coated pit imaged during its initiation phase. A step-fitting function (black) was used to determine the fluorescence intensity and dwell time (duration) associated with the first two steps (indicated by their respective numbers); these values were combined to generate the fluorescence intensity distribution shown in the gray histogram of (D).

(D) Data flow and computational analysis. Stage 1 shows the weighted contributions (green) for the calculated distribution of the number of EGFPs corresponding to different modes of triskelion recruitment (weights a_1 to a_3) constrained by the known molecular structures. For example, in the case of clathrin, EGFPs can only arrive in sets of one, two, three, etc., as part of one or more triskelions, each containing either zero, one, two, or three EGFP-LCa, and their relative amounts are weighted by the extent of light-chain replacement (B). Stage 2 shows the combined weighted distribution of numbers of EGFPs (blue) from stage 1 and the calculated EGFP distribution obtained by convolving the distribution of calculated EGFP molecules with Gaussians (light blue), for which the means and SDs were derived from the single-molecule calibration of fluorescence intensity. Calibrations are presented in Figure S1. Stage 3 corresponds to the comparison between the calculated EGFP intensity distribution (blue trace) and the experimentally determined EGFP measurements (gray). The number of clathrin triskelions recruited during a step is obtained by an iterative search process that minimizes the least-squares difference of the cumulative distribution functions between the experimentally measured and the calculated EGFP distribution values yielding the final weighted contribution and light-chain substitution parameters (stage 4). See also Figure S1.

to detect arrival of individual molecules (Kirchhausen, 2009; McMahon and Boucrot, 2011; Taylor et al., 2011; Traub, 2009). Molecular species clearly necessary to launch assembly of a committed coated pit at the inner plasma-membrane surface are clathrin and AP2s; PI-4,5-P_2 may be essential to bring AP2 to the membrane (Antonescu et al., 2011; Boucrot et al., 2006; Zoncu et al., 2007); and members of the rim complex are required at some early stage (Henne et al., 2010; Reider et al., 2009). Any ensemble measurement or any set of low-sensitivity imaging sequences is likely to obscure temporal sequences and potential causal relationships.

We describe here measurements that determine the sequence of initial events in individual coated structures (Figure 1). We used unbiased object detection and trajectory tracking to analyze live-cell TIRF images recorded with single-molecule enhanced green fluorescent protein (EGFP) detection and high temporal resolution. Because we could detect the arrival of individual clathrin triskelions and AP2 adaptors to sites of coated pit initiation (Figures 1A–1C), we could apply computational modeling to determine the stoichiometry of the protein complexes at early time points as well as the extent of substitution of endogenous by ectopically expressed fluorescently tagged chimeras (Figure 1D). We find that all pits initiate with two sequential events, and each event is usually a coordinated arrival of one triskelion and two AP2 complexes but is sometimes two triskelions and four AP2s. PI-4,5-P_2 is essential. FCHo1 and FCHo2 are not essential to initiate coated pit formation but rather to sustain growth of the clathrin coat and invagination of the membrane.

RESULTS

Recruitment of Clathrin to Coated Pits Detected with Single-Molecule Sensitivity

To study the molecular events during initiation of a coated pit at the cell surface, we first established that our TIRF microscope and our analytical tools (see Extended Experimental Procedures and Figure S1 available online) would allow detection of the fluorescence contributed to a diffraction-limited spot by a single EGFP. We imaged biotinylated EGFPs captured by avidin on the surface of a glass coverslip modified (to prevent nonspecific adsorption of protein) with an inert layer of biotinylated poly(ethylene glycol) (PEG) (Böcking et al., 2011). The decrement in a single photobleaching step of the intensity from a diffraction-limited spot (Figures S1A and S1B) obeyed a normal distribution, and we could take the average of that distribution as the

fluorescence signal from one EGFP (Figure S1C). We then found, as expected, that the intensity thus calibrated scaled linearly with the number of EGFP molecules captured within the spot (Figure S1D). We confirmed that EGFP association with triskelions or AP2 imaged on a nonmodified glass coverslip did not affect the amplitude of the photobleaching step by showing that the amplitude was the same whether EGFP was alone or fused to a triskelion-bound clathrin light chain LCa (EGFP-LCa) or fused to the AP2-bound adaptin σ2 (σ2-EGFP) (Figure S1E); clathrin and AP2 tagging were achieved by stable expression of EGFP-LCa and σ2-EGFP, respectively (Ehrlich et al., 2004; Loerke et al., 2011).

We used the TIRF setup thus calibrated with biotinylated EGFP to follow coated pit formation in BSC1 cells (Figure 1). Cells were allowed to attach to a layer of biotinylated fibronectin, which was bridged by avidin to the biotinylated PEG that coated the coverslip and provided an optically flat support. We confirmed that the clathrin-dependent endocytic activity was normal in cells attached to the modified PEG support by showing that plating onto the modified substrate had no effect on the kinetics of coat formation. This was determined by live-cell spinning-disk confocal microscopy of fluorescently tagged clathrin or AP2 imaged in the bottom and top surfaces of the cells and of uptake of fluorescently tagged transferrin (data not shown). Cells plated on the modified PEG support also had many fewer clathrin-coated plaques than did those attached directly to glass for 1 or more days (data not shown).

We acquired TIRF data at a frequency of ~5.5 Hz to provide an adequate number of data points and recorded for a total interval of 60 s to minimize photobleaching and potential phototoxicity (see for example Movie S1). The relatively short recording interval did not, in general, allow us to determine whether a growing clathrin-coated structure corresponded to a committed or an abortive pit (Ehrlich et al., 2004; Kirchhausen, 2009; Loerke et al., 2009; Saffarian et al., 2009), as the time series for most of them ended before complete assembly. We believe that this uncertainty has no effect on the conclusions we draw here because, during the initiation phase, the characteristics of clathrin and AP2 recruitment are the same, regardless of the duration of the event (Ehrlich et al., 2004; Loerke et al., 2011).

We identified all the fluorescent objects from five independent cells by using the u-track software package (Jaqaman et al., 2008). We selected events for analysis by applying the following criteria. (1) The fluorescent spot remained diffraction limited for the full duration of the time series. (2) The spot moved less than ~0.16 μm (2 pixels/frame) in x and y and did not collide with other fluorescent objects. These criteria selected plasma-membrane-bound pits and rejected structures associated with endosomal membranes that transiently approached the cell surface. (3) The spot was not present when the time series began and remained longer than 10 frames (1.7 s). This criterion eliminated transients and ensured that we included only true initiations. The fluorescence intensity of spots that met these criteria always increased with time (Figures 1C and 2A), which is a property established previously for both committed and abortive pits (Ehrlich et al., 2004; Loerke et al., 2009; Saffarian et al., 2009). The beginning of the trace was taken as the time point at which the net fluorescence intensity (over background) was equivalent to the signal from at least one EGFP (Figures 1C and 2A, right panels). We inspected the individual traces of all objects that lasted longer than 15 s and confirmed that the automated assignment of the starting point agreed with the time chosen "by hand" in over 80% of such events; the starting point for the remaining pits was adjusted manually so as to include the complete initiation phase.

Detailed analysis of clathrin traces for early phases of 537 coated pits from five cells showed that the first detectable events were two consecutive stepwise increases in fluorescence intensity (Figure 2A, right panels, selected examples). Histograms of the distribution of time intervals between the first and second intensity increments and between the second and subsequent ones, with average dwell times of 2.3 and 1.9 s, respectively, are in Figure 2B. The rise and fall, rather than single exponential behavior, of the distributions suggests that more than one rate-limiting step determines the kinetics of each of these two clathrin-recruitment events. The number of EGFP-LCa per clathrin triskelion can vary from zero to three, depending on the level of fluorescent light-chain expression and the degree of substitution for endogenous clathrin light chain a (LCa) and clathrin light chain b (LCb) (Figure 1B), and direct inspection indeed showed considerable variability in the magnitudes of the fluorescence increments. To determine the number of EGFP-LCa molecules recruited during each of the consecutive steps, we fitted the intensity distributions with different models that took into account variable degrees of light-chain substitution and alternative contributions of clathrin triskelions during the first and second steps of recruitment—for example, only one triskelion, only two triskelions, or a variable combination of one and two triskelions, etc. For each model and for each of the first two events, we calculated an expected EGFP frequency distribution based on the constraint that each event must correspond to arrival of one, two, or more triskelions, each with zero, one, two, or three EGFP-LCa, under the assumption that the EGFP-LCa occupancy follows a binomial distribution that depends on the ratio of ectopically expressed EGFP-LCa to endogenous LCa and LCb (see Experimental Procedures and Figure 1B). We varied both the relative fraction of events in which one, two, or more triskelions arrived at the plasma membrane and the extent of light-chain replacement (Figure 1D). From the EGFP frequency distribution associated with each model, we then calculated the associated EGFP intensity distribution by combining the corresponding Gaussians for which the means and SDs were given by the single-molecule calibration of fluorescence intensity (see Experimental Procedures and Figure 1D; see Figure 2C for all cells grouped together; and see Figure S2A for cells 1–5). We then calculated the number of clathrin triskelions recruited during each of the two events by minimizing the least-squares difference between the cumulative distribution functions of the calculated EGFP intensity for each model, determined as just described, and the experimentally determined EGFP measurements.

Selection of the best model was based on the Bayesian information criterion (BIC) (Jaqaman and Danuser, 2006; Schwarz, 1978) (see Experimental Procedures; Figure 2C). In the model that gave the best fit, ~75% of the events (either first or second step) corresponded to addition of a single clathrin triskelion, and

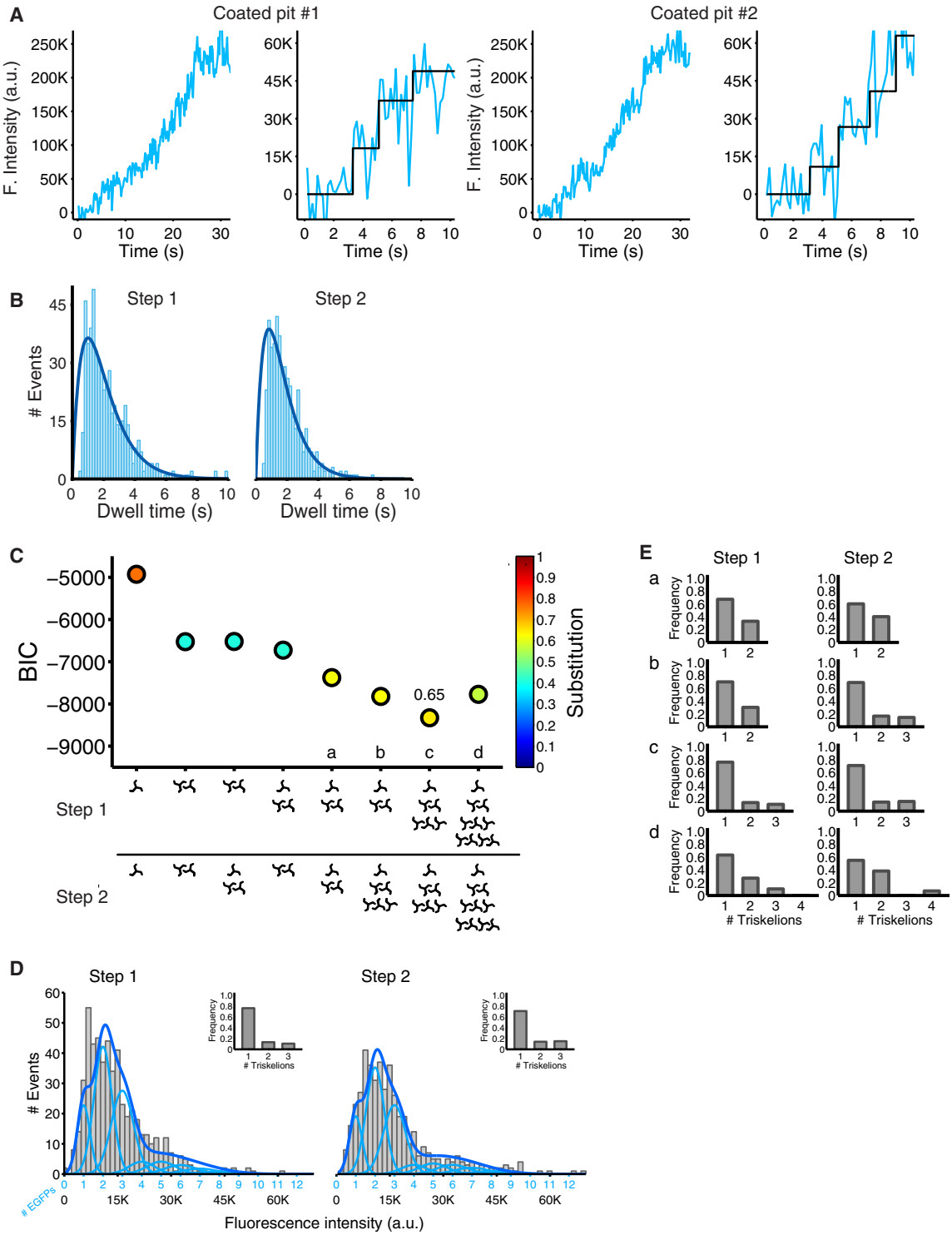

Figure 2. Recruitment of Clathrin during the Initiation Phase of Coated Pit Formation Detected with Single-Molecule Sensitivity

(A) Plot of the fluorescence intensity traces during the formation of two coated pits containing clathrin EGFP-LCa. The data were obtained from BSC1 cells stably expressing EGFP-LCa imaged by TIRF microscopy every 170 ms with an exposure of 30 ms per frame. The panels on the right are expanded traces corresponding to the first 10 s during the lifetime of the coated pits; they show the result of the fit (black) obtained by applying a step-fitting function to estimate the average fluorescence intensity and dwell time of the first two steps during the initiation phase of the pit.

(B) Distribution of dwell times of the first and second steps of clathrin EGFP-LCa recruitment during the initiation phase of coated pit formation. Data from 537 coated pits in five cells. The dark blue line is a fit of a simple model based on two rate-limiting molecular steps.

the remainder corresponded to addition of two or three triskelions (10%–15% of events each) (Figures 2C and 2D, BIC values for all cells combined and Figures S2A and S2B for individual cells 1–5). The best fit gave ~65% replacement of endogenous light chain by LCa-EGFP (Figure 2C for all cells and Figure S2D for cells 1–5), which was in excellent agreement with the experimental value of ~60% from conventional western blot analysis of a large pool of cells (Figure S2E). For some other models, the quality of the fit was similar to that for the best model (Figure 2C, models a–d); in these models, a single triskelion also arrived in ~75% of the events, but the remaining events corresponded to variable arrival of small amounts of two or three triskelions (Figure 2E). We obtained very poor fits with calculations that assumed significantly different recruitment models or different replacement levels (Figure 2C for all cells grouped together and Figure S2A for cells 1–5).

The analysis thus suggests that coated pit formation generally begins with arrival of a single triskelion at each of two successive recruitment steps and that coincident arrival (within the ~170 ms time resolution of our measurements) of two or three triskelions can also occur but with much lower probability. These initial steps are then followed by more rapid recruitment of many additional triskelions. We established the robustness of the analysis used to determine how coated pit assembly starts by performing the calculations just described on simulated "noisy" image sequences (movies) corresponding to clathrin recruitment during coated pit formation (see Analytical Validation in Extended Experimental Procedures and Figure S3).

Recruitment of AP2 to Coated Pits Detected with Single-Molecule Sensitivity

We investigated recruitment of AP2 tagged with σ2-EGFP during initiation of coated pit formation by using the same approach with which we detected the early arrival of clathrin (see Movie S2). We use the cell-attachment and TIRF imaging conditions described above for the clathrin-recruitment experiments. We recorded data from 698 coated pits in six different cells. As for clathrin, we detected two well-defined, stepwise increments in fluorescence intensity (Figure 3A, two pits shown as examples), with average times between successive increments of 2.6 and 2.2 s, respectively. The distributions for these intervals (Figure 3B) were the same as those for the intervals between initial clathrin recruitments (Figure 2B) ($p > 0.2$, step 1; $p > 0.12$, step 2; Kolmogorov-Smirnov test [KS-test]), indicating that the two processes are related. The distribution of dwell times between the first recruitment steps of clathrin or AP2 showed a rise-and-fall profile that was consistent with more than one rate-limiting event rather than following an exponential decay that would be consistent with a single rate-limiting step (see Analytical Validation in Extended Experimental Procedures and also Figure S4).

We used a Gaussian mixture model, as above, to determine for each cell the distribution of intensity increments associated with each of the two recruitment events (Figure 3C for all cells grouped together and Figure S5A for cells 1–6). There is one σ2-EGFP per AP2 heterotetramer, so the distribution of EGFP intensities corresponds directly to the distribution of tagged complexes. The distributions showed a strong preference for two AP2 complexes per event in the first and second increments (Figure 3D, insets, for all cells grouped together and Figure S5B for cells 1–6).

We fitted the experimental AP2 distribution data with a recruitment model similar to the one described above for clathrin triskelions. In the best fit (model d), two AP2 complexes arrive together in 80% and 60% of the events in the first and second steps, and four or six (e.g., two or three pairs) arrive in the remaining 20%–40% (Figures 3D and 3E, inset for all cells grouped together and Figure S5B for cells 1–6). We tested a large number of other models, all of which gave significantly poorer fits (Figure 3C for all cells together and Figure S5C for cells 1–6). Models a, b, c, and e were not very different from each other, and in every case the common feature was the favored arrival of two AP2s. We varied the degree of endogenous σ2 replacement by σ2-EGFP and searched for the best fit consistent with the experimental frequency distributions. The calculated replacement value was ~84% (Figures 3C and 3E for all cells and Figure S5D for cells 1–6), which was in excellent agreement with the ~80% replacement determined experimentally by western blot (Figure S5E). Analytical validation for these procedures is provided in Extended Experimental Procedures (see also Figure S6). We further tested the consistency of our models by adding constraints derived from fitting the clathrin arrival distributions (75%, one triskelion; 25%, two and three triskelions, Figure S7). The latter distributions yielded a good fit to the AP2 distributions, giving an estimate that, during the initial event, 90% of the triskelions arrived with two bound AP2 complexes. Because we did not know how many AP2 were "dark" (untagged) during any specific step in growth of an individual pit, we could not determine whether there was any correlation between the number of AP2 complexes (or clathrin triskelions) in the first and second recruitment events.

(C) Value of the BIC used to determine the best fit between the experimental data and the recruitment models of clathrin indicated at the bottom. The quality of the fit increases with more negative BIC values (see Experimental Procedures; Schwarz, 1978). Each point was color coded according to the calculated substitution level of endogenous light chain by the ectopically expressed EGFP-LCa. The relative contributions of triskelions in models a–d are presented in (E).

(D) The compiled distribution of net fluorescence intensities (fluorescence intensity for a given spot minus the fluorescence intensity of the background, in arbitrary units) of recruited clathrin EGFP-LCa was determined for the first and second steps during the initiation phase of all pits in the five cells analyzed (gray). The continuous fluorescence intensity signal (dark blue) is the sum of the relative contributions to the fluorescence signal by the incorporation of one, two, etc., EGFP molecules (light blue) that were obtained from the model with the best BIC score (panel C, model c). For the first step, the model represents the arrival of a single triskelion in ~75% of the events and two and three triskelions in the remaining ~25% (inset). For the second step, the model represents the arrival of one, two, and three triskelions in ~70%, ~14%, and ~16% of the events, respectively (inset). The calculated extent of endogenous light-chain substitution for all cells with EGFP-LCa was 65%.

(E) Arrival of triskelions to the first and second steps of the models a–d highlighted in (C). The gray histograms show the relative contributions of triskelions recruited in the first and second steps of clathrin-coated pit formation for the three models (a, b, and d) with a BIC score closest to the best model (c).

The analyses of the single cells are reported in Figure S2 for cells 1–5. See also Figures S3 and S7 and Movie S1.

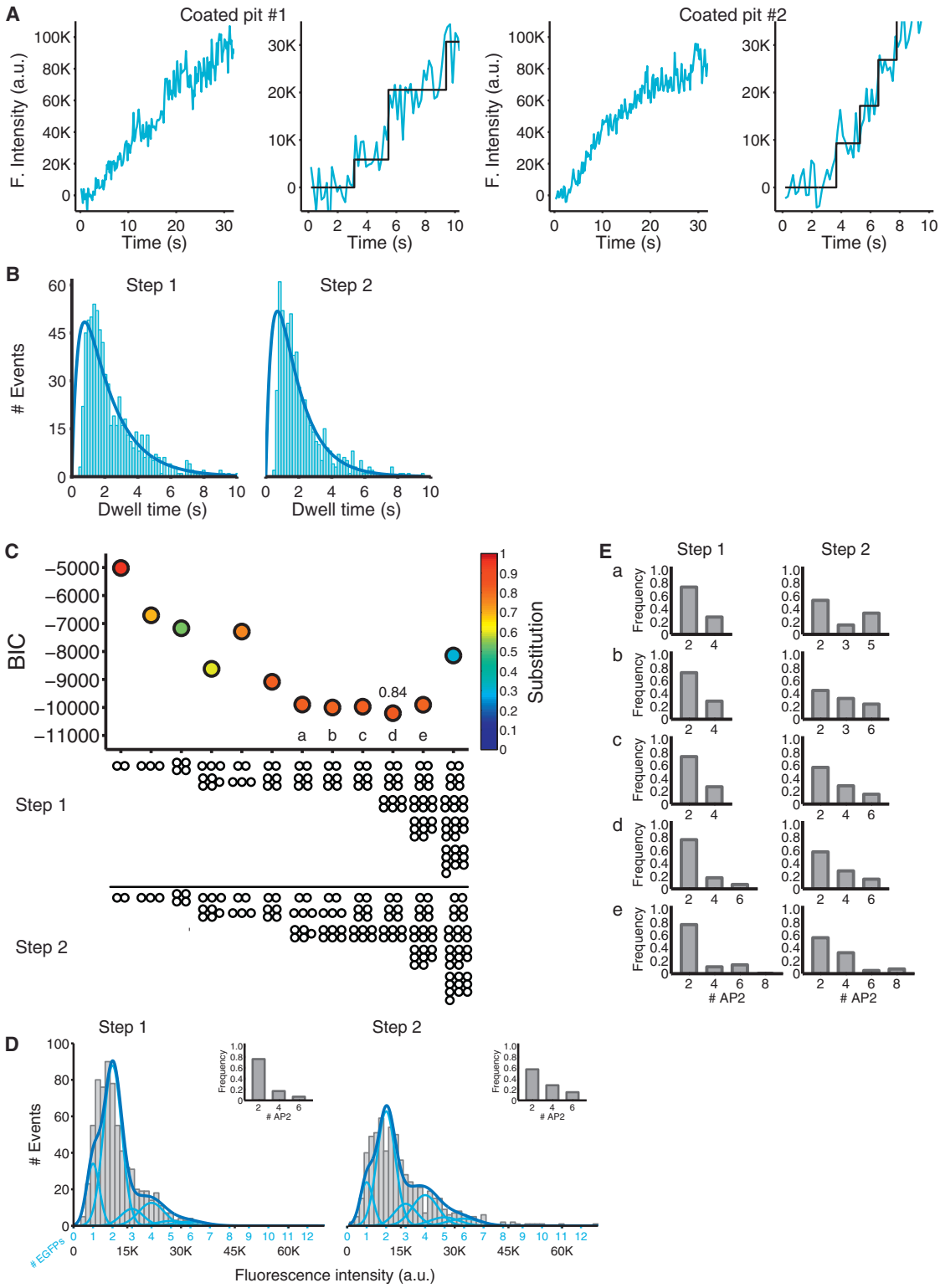

Figure 3. Recruitment of AP2 during the Initiation Phase of Coated Pit Formation Detected with Single-Molecule Sensitivity

(A) Plot of the fluorescence intensity traces during the formation of two coated pits containing AP2 tagged with σ2-EGFP. The data were obtained from BSC1 cells stably expressing σ2-EGFP imaged by TIRF microscopy every 170 ms with an exposure of 30 ms per frame. The panels on the right are expanded traces corresponding to the first 10 s during the lifetime of the coated pits; they show the result of the fit (black) obtained by applying a step-fitting function to estimate the average fluorescence intensity and dwell time of the first two steps during the initiation phase of the pit.

Joint Recruitment of Clathrin and AP2 for Coated Pit Initiation

The strong correlation between the distributions of time intervals between initial steps of clathrin recruitment and AP2 recruitment and the fit of the constrained model just described both suggest that clathrin and AP2 arrive as partners. We therefore adapted our TIRF configuration to image EGFP and mCherry in the same experiment, thus allowing us to follow recruitment of σ2-EGFP and mCherry-LCa to the same coated pit. We used BSC1 cells, stably expressing σ2-EGFP, that had been transfected 48 hr before the experiment with a plasmid-encoding mCherry-LCa and modified the microscope to allow simultaneous dual-wavelength excitation and detection of both fluorophores. We verified absence of crosstalk between the two emitted signals. The two intensities were expressed as relative values to each other because mCherry photobleaches quite rapidly, making it impractical to obtain an absolute fluorescence intensity calibration relative to single mCherry.

The representative traces in Figures 4A and 4B show clear correlation of fluorescence from clathrin and AP2, particularly during the early stage of coat assembly. The distribution of the difference between times of initial clathrin and AP2 signals is a Gaussian centered on 0 s, suggesting that, within the time resolution of our experiments (170 ms), the two species arrive together (Figure 4C). Uncertainties in identifying the beginning of the first step due to the inherently noisy fluorescence intensity data from cells simultaneously expressing σ2-EGFP and mCherry-LCa are likely to explain the distribution of observed timing differences because similar distributions were obtained by using simulated traces generated with the same signal-to-noise ratio (data not shown). Another potential source for the observed uncertainty is coordinated arrival of untagged AP2 with tagged clathrin or the converse; the proportion of tagged AP2 would have been lower because of low expression of σ2-EGFP in cells transiently expressing LCa-mCherry driven by the same promoter (E.C. and T.K., unpublished data).

Role of FCHo1 and FCHo2 in Coated Pit Initiation

It has been proposed that FCHo1 and FCHo2 are required for coated pit initiation because pits fail to form in their absence (Henne et al., 2010). One line of evidence is absence of AP2-containing pits on the attached plasma membrane of cells imaged by spinning-disk confocal microscopy after depletion of both FCHo1 and FCHo2 by RNA interference (RNAi) (Henne et al., 2010). We reproduced this observation by using small hairpin RNA (shRNA) with the published depletion protocol and the same σ2-EGFP-expressing BSC1 cells. We confirmed the absence of AP2 puncta at the cell surface and enhanced cytosolic AP2 fluorescence background (Figures 5A and 5B); the positive control from cells expressing FCHo1/2 at normal levels showed normal AP2 puncta and lower cytosolic background. A quantitative comparison showing loss of coated vesicles in the absence of FCHo1/2 is shown in Figure 5C. As others have found by using spinning-disk confocal imaging (Henne et al., 2010), we observed loss of receptor-mediated endocytosis of transferrin in cells depleted of both FCHo1 and FCHo2. By using spinning-disk confocal imaging, we found that, in cells lacking AP2 puncta, Alexa647 transferrin failed to internalize and accumulate in endosomes (Figure 5A). Fluorescence-activated cell sorting (FACS) analysis confirmed the partial loss of transferrin uptake in cells subjected to FCHo1/2 depletion (Figure 5D). The partial effect is in line with the extent of protein depletion determined by western blot analysis (Henne et al., 2010; Nunez et al., 2011) and is consistent with an ~50% efficacy of FCHo1/2 depletion determined by real-time quantitative PCR (qtPCR) (data not shown).

The sensitivity of the spinning-disk confocal microscope is insufficient, however, to detect the weak fluorescent signals associated with a small number of fluorescent molecules. We therefore used the more sensitive TIRF imaging to determine whether or not FCHo1/2 are required for AP2 recruitment during the initial phases of coated pit formation described above. We found a substantial reduction in the number of longer-lived AP2 spots (lifetimes >25 s) in the FCHo1/2-depleted cells but no decrease in the number of shorter-lived spots (lifetimes <10 s) (Figures 5E and 5F). The latter are abortive pits that fail to proceed to complete assembly and pinching. We included two negative controls to ensure that the short-lived events are bona fide AP2 pits rather than collisions of cytosolic AP2 with the plasma membrane. In one experiment, we showed total absence of AP2 events in cells treated briefly with 1-butanol (Figures 5E and 5F), a procedure that completely eliminates formation of clathrin/AP2-coated pits (Boucrot et al., 2006; Henne et al., 2010). In the other, we showed absence of detectable random association of EGFP with the plasma membrane in cells expressing cytosolic EGFP rather than σ2-EGFP (Figures 5E and 5F).

(B) Distribution of dwell times of the first and second steps of AP2 σ2-EGFP recruited during the initiation phase of coated pit formation. Data from 698 pits in six cells. The dark blue line is a fit of a simple model based on two rate-limiting molecular steps.

(C) Value of the BIC used to determine the best fit between the experimental data and the recruitment models of AP2 indicated at the bottom. The quality of the fit increases with more negative BIC values. Each point was color coded according to the calculated substitution level of endogenous σ2 by the ectopically expressed σ2-EGFP. The relative contributions of AP2 recruitment in models a–e are presented in (E).

(D) The compiled distribution of net fluorescence intensities (fluorescence intensity for a given spot minus the fluorescence intensity of the background, in arbitrary units) of recruited AP2 σ2-EGFP was determined for the first and second steps during the initiation phase of all pits in the six analyzed cells (gray). The continuous fluorescence intensity signal (dark blue) is the sum of the relative contributions to the fluorescence signal by the incorporation of one, two, etc., EGFP molecules (light blue) that were obtained from the model with the best BIC score (panel C, model d). For the first step, the model represents the arrival of two AP2 in ~75% of the events and four and six AP2 in the remaining ~25% (inset). For the second step, the model represents the arrival of two, four, and six AP2 in ~55%, ~30%, and ~15% of the events, respectively (inset). The calculated extent of endogenous σ2 substitution with σ2-EGFP was 84% for all cells.

(E) Arrival of AP2s to the first and second steps of the models a–e highlighted in (C).

The gray histograms show the relative contributions of AP2 recruited in the first and second steps of clathrin-coated pit formation for the four models (a–c and e) with a BIC score closest to the best model (d).

The analyses of the single cells are reported in Figure S5 for cells 1–6. See also Figures S4, S6, and S7 and Movies S2 and S3.

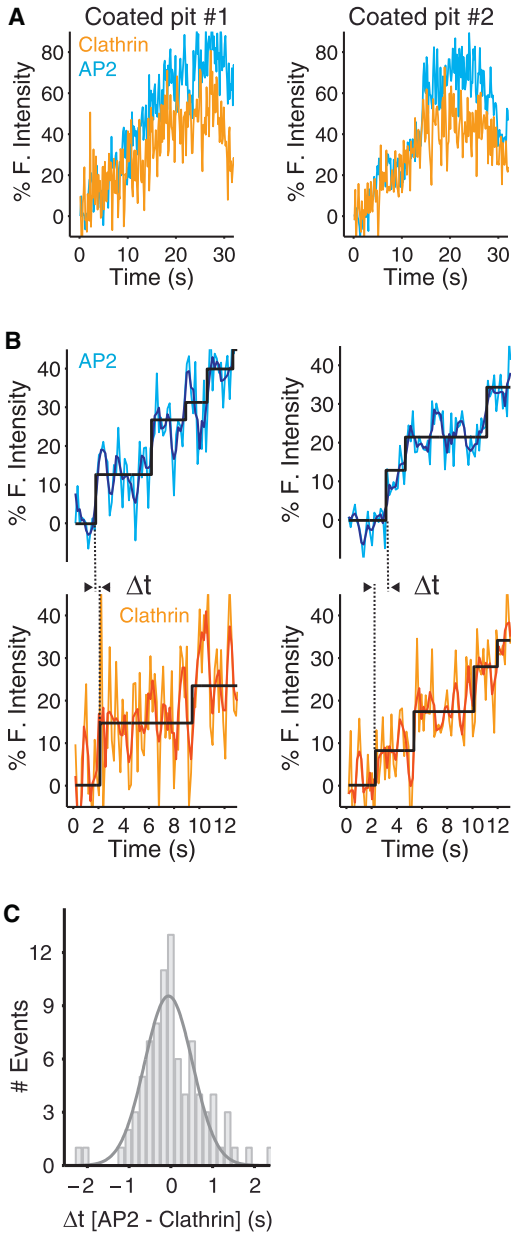

Figure 4. Recruitment of Clathrin and AP2 during the Initiation Phase of the Same Coated Pit

(A) Fluorescence intensity traces corresponding to the recruitment of clathrin and AP2 during the formation of two coated pits containing clathrin mCherry-LCa and σ2-EGFP. The data were obtained from BSC1 cells stably expressing σ2-EGFP and transiently expressing mCherry-LCa. The cells were imaged by TIRF microscopy with the dual view setup every 170 ms with simultaneous excitation of mCherry and EGFP using exposures of 30 ms per frame. The traces correspond to the first 30 s during the lifetime of the coated pits.

(B) The expanded traces show the raw fluorescence signals (light blue, light orange); the corresponding smoothened plots (dark blue and red) were obtained with a running average filter (window size = 3). The fitted steps (black) obtained by applying the step-fitting function to the raw signals were then used to measure the dwell time of the first step and to determine the difference in the arrival time (Δt) of AP2 and clathrin during the first step.

(C) Distribution of the difference in the arrival time (Δt) of clathrin mCherry-LCa and AP2 σ2-EGFP during the initiation step of 83 coated pits from five cells.

We also used TIRF imaging to characterize the dynamics of pit formation in BSC1 cells overexpressing untagged FCHo1 and stably expressing σ2-EGFP. Although there was no significant increase in the total number of initiation events (e.g., AP2 spots with lifetimes >2 s, Figure 5G), we found a clear increase in the number of longer events—that is, those lasting between 5 and 25 s (Figure 5H). A fraction of these 5–25 s events probably represent fully formed coated pits that assembled more rapidly because their AP2 content was equivalent to that of committed pits that took 40 s or more to form. In addition, FCHo1 overexpression led to a noticeable decrease of abortive events lasting between 2 and 5 s. We conclude that, although FCHo1/2 are clearly important for ensuring growth and completion of the coat, they are not essential for coated pit initiation. We propose instead that the FCHo molecules are part of a larger complex that stabilizes the assembling coat, allowing further growth of the clathrin lattice.

DISCUSSION

Our experimental analysis of the first 5 s of clathrin-coated pit assembly leads to the following molecular description (Figure 6). There are two early recruitment events that we can resolve here, followed in rapid succession by additional recruitment of clathrin and AP2 in steps that we cannot resolve. The two early events include both AP2 and clathrin, which arrive together at the site destined to become a coated pit. The molecular description of a majority of the recruitment events (both first and second) is one clathrin triskelion and two AP2 complexes; in a smaller fraction of the events, two triskelions and four AP2s participate. This description clearly rules out the alternative notion inferred from cells partially depleted of clathrin that triskelions assemble on a preformed patch of AP2 (Hinrichsen et al., 2006).

Coordinated Arrival of One Triskelion and Two AP2 Complexes

The most straightforward explanation of the observed stoichiometry is that only if two AP2 complexes anchor clathrin to the membrane will its lifetime there be long enough to allow subsequent addition of more clathrins. This interpretation is consistent with known properties of the components. AP2 binds weakly but specifically to lipid bilayers (such as the plasma membrane) that contain PI-4,5-P_2; clathrin has no direct membrane contacts. Once a lattice has begun to form, clathrin-clathrin contacts will add stability and will greatly increase the mean residence time, both for clathrin and for the AP2 complexes it binds. Each of the two resolvable, early addition events includes more than one rate-limiting molecular step. The rise-and-fall shape of the dwell-time histogram leads to this conclusion, even without a specific molecular picture. It is not yet clear, however, which of the steps implied by the stoichiometry just described determine the observed kinetics.

A full analysis has required a model that explicitly incorporates the degree of substitution of untagged components by tagged ones, the distribution of light-chain occupancies, and the distribution of the number of clathrin trimers that contribute to each event. In the case of clathrin, each triskelion has three light chains at equivalent sites occupied randomly by LCa and LCb.

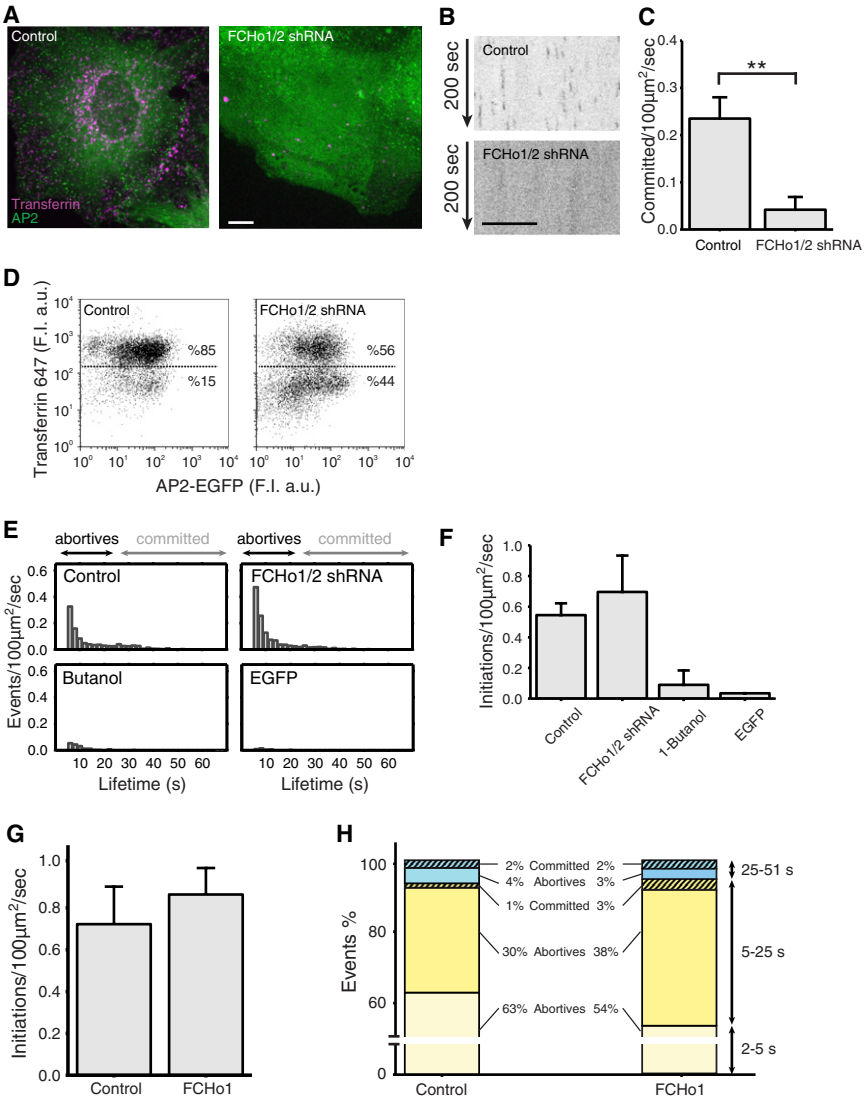

Figure 5. Effect of FCHo Proteins on Coated Pit Initiation and Formation

(A) Uptake of Alexa 647 transferrin (magenta) by BSC1 cells stably expressing σ2-EGFP (green) in the presence and absence of FCHo1 and FCHo2. Depletion of FCHo1/2 was obtained after a 4 day incubation with lentivirus encoding short-hairpin interfering RNA sequences specific for FCHo1 and FCHo2 (FCHo1/2 shRNA). Cells were incubated for 10 min at 37°C with 10 μg/ml Alexa 647 transferrin and then imaged in 3D using spinning-disk confocal microscopy. The representative images correspond to maximum z projections from a stack of 35 imaging planes spaced 0.5 μm. Scale bar, 10 μm for both panels.

(B) Representative kymographs from time series from the bottom attached surface of BSC1 cells obtained by spinning-disk confocal microscopy. The cells stably expressing σ2-EGFP were imaged in the presence (top) or absence (bottom) of FCHo1/2. Time series were obtained 4 days after treatment of the cells with lentivirus encoding scrambled or short-hairpin interfering RNA sequences specific for FCHo1 and FCHo2. Scale bar, 10 μm for both panels.

(C) Distributions of the numbers of coated pits longer than 25 s forming in the presence (0.23 ± 0.045 committed pits/100 μm^2/s; total number of pits = 3,275) and absence (0.042 ± 0.027; total number of pits = 1,139) of FCHo1/2. Error bars represent cell-to-cell SD; $^{**}p < 10^{-4}$, t test. Data from five cells for each condition.

(D) FACS analysis to follow the uptake of Alexa 647 transferrin by BSC1 cells stably expressing σ2-EGFP in the presence (left) and absence (right) of FCHo1/2.

(E) Number of coated pit events detected by TIRF in the presence and absence of FCHo1/2, respectively. Time series were obtained by imaging every 170 ms with an exposure of 30 ms per frame. The number of committed pits (>25 s) was underrepresented because the length of the time series used was 1 min in duration.

(F) Distributions of fluorescent spots representing the number of initiation events with duration longer than 5 s detected by TIRF microscopy in BSC1 cells stably expressing σ2-GFP; 51 s time series were obtained by imaging every 170 ms with an exposure of 30 ms per frame. The data were obtained from control cells expressing normal amounts of FCHo1 and FCHo2 (0.544 ± 0.076 initiations/100 μm^2/s; n = 4 cells), from cells depleted of FCHo1 and FCHo2 (0. 696 ± 0.23; n = 3 cells), and from control cells briefly exposed to 1-butanol (0.089 ± 0.094; n = 3 cells). The last bar shows the distribution of fluorescent spots detected at the plasma membrane of cells expressing soluble cytosolic monomeric EGFP (0.034; n = 1 cell). Error bars represent SD.

(G) Distributions of the numbers of fluorescent spots representing initiation events (>2 s) detected by TIRF microscopy in BSC1 cells stably expressing σ2-GFP alone or together with transiently expressed FCHo1. We recorded 51 s time series by imaging every 170 ms with an exposure of 30 ms per frame. The data were obtained both from control cells expressing normal amounts of FCHo1/2 (0.722 ± 0.179; n = 5 cells) and from cells transiently expressing FCHo1 for 3 days (0.864 ± 0.126; n = 5 cells). Error bars represent SD.

(H) The events detected in (G) were divided into three groups: those lasting 2–5, 5–25, and 25–51 s. The data are color coded to differentiate abortive (full color) from committed pits (striped), and the later were selected by their higher maximum fluorescence intensity.

Thus, depending on the level of expression of the tagged LCa, a triskelion might have between zero and three fluorophores. Our data show discernable arrival of up to nine EGFPs in each of the first two events. Assuming stochastic replacement of endogenous light chains with the ectopically expressed LCa-EGFP, we searched for the best correlation of observed and modeled binomial frequency distributions with the degree of replacement as a variable. For clathrin, we found the best fit with a single triskelion in 75% of the events and two or three in the remaining 25%, with an overall replacement of 65% of the light chains with EGFP-LCa. For AP2, we detected steps of between one and four clathrin adaptor complexes and a strong preference for two. A step with a single AP2 could be arrival of a pair with one of the complexes untagged (i.e., bearing endogenous σ2). A global fit with different binomial models converged to one in which two AP2 complexes arrived together in ~80% of

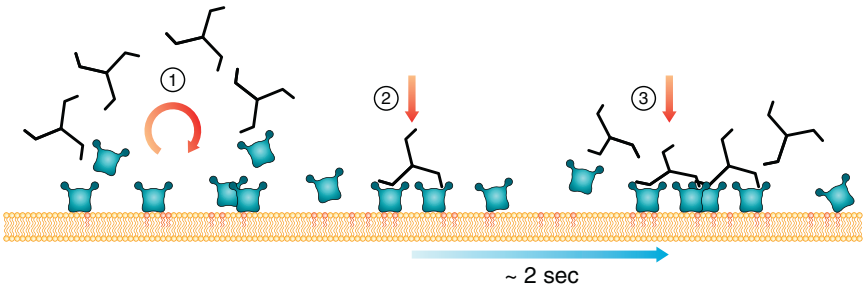

Figure 6. Proposed Model for Recruitment of Clathrin and AP2 during the First Five Seconds of Coated Pit Formation

Schematic representation of the early events during initiation of coated pit formation. (1) AP2 binds weakly to PI-4,5-P_2 contained in the plasma membrane, leading to rapid association and dissociation. Clathrin has no affinity for the membrane, and interactions between clathrin and a single AP2 are also too weak to form a stable complex. (2) The first recognizable event coordinated binding of a clathrin triskelion to two membrane-anchored AP2s; the two anchor points stabilize the resulting complex and increase its residence time at the membrane. (3) The increased residence time of the triskelion/AP2 complex results in the second resolvable event, incorporation of a further building block, typically consisting of one triskelion bound to two AP2s. In a small proportion of cases (~30%), the incorporation rate of a second triskelion/AP2 complex is faster than the temporal resolution of data acquisition (170 ms), resulting in the combined model of 70% one triskelion/2 AP2 + 30% two triskelions/4 AP2 in steps one and two. The accessory proteins FCHo1 and FCHo2 are not involved in the initial two steps of assembly.

the events and four or six AP2 complexes in the rest, with about 80% overall replacement of endogenous σ2 by σ2-EGFP. We found no evidence for preclustering of AP2 before arrival of clathrin.

The models for clathrin and AP2 recruitment yield replacement levels in excellent agreement with the values measured directly by western blots from pooled-cell extracts. Moreover, when we constrain the AP2 recruitment model by the best fit of the clathrin model—75% of the events with a single triskelion and 25% with two or three—and allow each triskelion to arrive with one, two, or three associated AP2 complexes, the best fit converges to a strong preference for two AP2s per step and to essentially the same replacement values as in the unconstrained calculation. We further validated the analytical method used to determine the first steps of clathrin and AP2 recruitment leading to coated pit formation by showing that the method returned the same values as those input to models used to generate movies simulating coated pit formation.

Single-molecule sensitivity in our measurements has been critical for the robustness of the modeling just described and for the excellent agreement the models yield with experimentally determined replacement levels of endogenous by tagged components. To achieve single-molecule detection in live-cell imaging without resorting to quantum dots or other large clusters of fluorophores (Howarth et al., 2008; Howarth and Ting, 2008), we needed to make a number of improvements in cell handling, microscope hardware, and data analysis. Attaching cells to a layer of biotinylated fibronectin bridged by avidin to a coating of biotinylated PEG allowed access to the cell surface facing the coverslip, minimized background, and essentially eliminated formation of coated plaques. Improvements in temperature control and z axis stability of the microscope stage and use of TIRF illumination from an intense and stable laser source have allowed us to record signals from single EGFP molecules that are ~3 ± 0.7 SDs above cellular background in 30 ms exposures (calculation done by using the AP2 data from all six cells). The corresponding statistical significance ($p > 0.08 \pm 0.035$, t test) increases if subsequent time points have measurable signal for the same object ($p < 0.05$ after 2 ± 1 frames). Moreover, rapid recording—170 ms intervals in our work—enhances the stringency of the criteria we can apply for the maximum displacement between frames and the minimum number of frames in which the object appears. Calibration of the fluorescence intensity by photobleaching of immobilized EGFP allowed us to make a direct correspondence between signal strength and number of molecules contributing to any event we detected.

FCHo1 and FCHo2 Are Not Essential to Initiate Coated Pit Formation

The experiments described here illustrate the importance of imaging with single-molecule sensitivity when studying processes, such as initiation of assembly, that involve a very small number of components and the stochasticity that small numbers inevitably imply. Access to information about the distribution of molecular contributions to the events being analyzed avoids ambiguities inherent in ensemble measurements and isolated snapshots. Our reanalysis of the effect of ablating FCHo1/2 or overexpressing FCHo1 shows that methods (such as spinning-disk confocal imaging with conventional illumination) requiring extrapolation from later time points and stronger signals may lead to incorrect inference. FCHo1/2 are clearly necessary for coated pit assembly and clathrin-mediated endocytosis of transferrin (Henne et al., 2010), but we have shown that knockdown of these components does not affect initiation. Instead, we find that normally initiated coated pits abort in the absence of FCHo1/2 and that a fraction of coated pits assemble even faster than usual in the presence of large amounts of FCHo1. We propose that FCHo1/2 are part of a complex that stabilizes the nascent coated pit and permits or facilitates continued growth.

When FCHo1 is overexpressed, the fraction of fully formed committed coated pits increases, and often they assembled more rapidly, with a noticeable decrease of abortive events. When FCHo proteins are missing, coated pits abort assembly, typically 20–25 s after arrival of the initial clathrin and AP2s. The average lifetime of coated pits in the BSC1 cells studied here is 45–60 s; once pit assembly has initiated, clathrin adds at a relatively steady rate, so that 20–25 s would correspond to a pit with a roughly hemispherical coat. The critical stage at which FCHo1/2 and their partners are essential for coat assembly is therefore near the point at which the invaginated membrane starts to constrict. We have shown recently that

pits forming on membranes under tension require rescue at this stage (by actin polymerization) because the net free energy of membrane deformation begins to increase as constriction proceeds (Boulant et al., 2011). Thus, by stabilizing the growing coat, the FCHo proteins and their partners could allow continued growth to overcome increasing membrane resistance. The mechanism could involve stabilizing a curved membrane or reinforcing the clathrin lattice. The FCHo proteins associate with intersectin, epsin, and Eps15 (Henne et al., 2010). They have an F-BAR domain, which associates preferentially with curved membranes; the epsin N-terminal homology (ENTH) domain has a similar preference. Eps15, Epsin, and FCHo proteins are present selectively at the rim of an assembling coat (Henne et al., 2010; Saffarian et al., 2009; Tebar et al., 1996). FCHo1/2 and epsin might therefore stabilize bilayer curvature as the pit invaginates or simply recognize membrane curvature as part of a mechanism that stabilizes (directly or indirectly) the clathrin coat itself.

Model for Coated Pit Initiation

The observed recruitment kinetics suggests the following model for association of clathrin and AP2 in coated pit initiation (Figure 6). Cytosolic AP2s are constantly sampling membranes. Association of AP2 and PI-4,5-P_2 at a specific site on the α-subunit favors capture of AP2 at the plasma membrane, but the affinity for the lipid head group is relatively weak, and the residence time, in the absence of further interaction, is probably much less than 1 s. A single clathrin-AP2 contact or a single AP2-membrane-cargo protein association is also weak and comparably short lived. If, however, a membrane-associated AP2 binds a clathrin triskelion that recruits or brings with it an additional AP2, which can associate with a second PI-4,5-P_2 in the membrane, the three-component cluster (one triskelion and two AP2 complexes) will then have a much longer membrane residence time. We propose that this sort of cluster describes the most probable initial molecular complex, which is stable (in general) for the $\sim$1.7 s required for recruitment of a second clathrin. Because a single clathrin-clathrin interaction is weak (Fotin et al., 2004), stable association of the second clathrin will in most cases also require that it have two bound AP2 complexes. The stability and multiple valencies of the resulting structure will then permit a number of alternative molecular steps—e.g., recruitment of cytosolic clathrin with no bound AP2s, recruitment of an additional AP2 to one of the unoccupied terminal domains, etc.

Our description of initiation is an "average" of most probable sets of steps, not a proposal for a unique molecular sequence. Our model includes three central participants: AP2, PI-4,5-P_2, and clathrin. A crucial role for PI-4,5-P_2 follows from our observation that loss of this phosphoinositide from the plasma membrane after acute treatment of cells with 1-butanol prevents formation of any new coated pits. Our earlier work (Boucrot et al., 2006, 2010) and that of others (Henne et al., 2010; von Kleist et al., 2011) has shown that coated pits are absent in cells depleted of PI-4,5-P_2; our current data show that even the initial molecular recruitment steps fail to occur. We also see no evidence for association of clathrin-free AP2 with sorting motifs on the cytosolic extensions of membrane-resident cargo, as this interaction, together with binding of PI-4,5-P2, would greatly increase the residence time of clathrin-free AP2, which is contrary to our observations. Association with clathrin activates AP2, switching the μ2 subunit into its "open" conformation (Rapoport et al., 1997) and enhancing the likelihood of cargo capture once coat assembly is underway. This mechanism is consistent with observations that show capture of LDL (Ehrlich et al., 2004), transferrin (E.C. and T.K., unpublished data), and several types of viruses (Cureton et al., 2012; Ehrlich et al., 2004) to previously initiated assembling pits, rather than cargo-induced ab initio pit formation.

We have tagged with fluorescent reporters only the clathrin and AP2 components of a coat. Other proteins could, in principle, participate in the initiation steps we have followed. The most important mechanistic reason for a specific heterologous initiator of any assembly process is to guarantee inclusion of a particular component. Subsequent recruitment steps can also have this function, however. We have ruled out a requirement for FCHo1/2 as initiators, showing instead that they prevent assembly from aborting after 15–20 s; they could therefore direct incorporation of further components essential for later events, such as fusion of the uncoated vesicle with a target membrane. We note that a model invoking stochastic initiation, followed by molecular associations that commit the coat to complete its assembly, is more consistent with the large body of observations that have accumulated since our early live-cell imaging studies (Ehrlich et al., 2004) than is a model invoking a heterologous initiator.

EXPERIMENTAL PROCEDURES

Cell Biology

All of the procedures used for cell biological manipulations are described in detail in the Extended Experimental Procedures.

Visualization and Image Analysis

Samples were visualized by using TIRF microscopy with single-molecule EGFP detection and high temporal resolution or spinning-disk confocal fluorescence microscopy with high temporal resolution. Coated pits were detected and tracked by using the u-track software (Jaqaman et al., 2008). The objects thus selected were analyzed further by using additional software written in Matlab (Mathworks, Natick, MA). We only considered for analysis those objects whose fluorescence intensity increased with time, appeared after the time series started, moved less than 0.16 μm/frame along the x and y axis (the average of the movement was 0.41 pixel/frame, and the median was 0.28 pixel/frame), and did not collide with other fluorescent objects. Fluorescence intensity traces during the first 10 s of clathrin or AP-2 recruitment thus obtained were fitted by using a step detection function (Smith, 1998) to define the intensity and the dwell time of the molecule incorporation at the nascent coated pits. To quantify protein recruitment, the cumulative distributions of intensities of the first and second steps of coated pit formation for all pits in each cell were together fitted with a model incorporating different combinations of protein recruitment as well as the extent of substitution in the cell, i.e., the probability q of a fluorescent molecule being incorporated. Detailed procedures, including simulations, are described in the Extended Experimental Procedures.

SUPPLEMENTAL INFORMATION

Supplemental Information includes Extended Experimental Procedures, seven figures, and three movies and can be found with this article online at http://dx.doi.org/10.1016/j.cell.2012.05.047.

ACKNOWLEDGMENTS

This work was supported by NIH grant GM-075252 (T.K.), a GlaxoSmithKline Fellowship (E.C.), a Swiss National Science Foundation fellowship (F.A.) and partial support from NIH grant GM-073165 (to G. Danuser, Harvard Medical School) (F.A.), and a Harvard Digestive Disease Consortium Feasibility Award (S.B.). We thank E. Marino (supported by NIH grant U54 AI057159, New England Regional Center of Excellence in Biodefense and Emerging Infectious Diseases) for maintaining the imaging resources, G. Findlay for qtPCR determinations, Janet Iwasa for the graphical abstract, and S.C. Harrison for editorial assistance. We gratefully acknowledge G. Danuser, K. Jaqaman, S.C. Harrison, and members of the Kirchhausen lab for thought-provoking discussions. E.C. and T.K. designed experiments; E.C. and S.B. performed experiments; E.C. and F.A. designed and implemented the computational methods; and E.C. and F.A. analyzed data. E.C., F.A., and T.K. discussed the results and contributed to the final manuscript.

Received: August 27, 2011
Revised: January 12, 2012
Accepted: May 31, 2012
Published: August 2, 2012

REFERENCES

Antonescu, C.N., Aguet, F., Danuser, G., and Schmid, S.L. (2011). Phosphatidylinositol-(4,5)-bisphosphate regulates clathrin-coated pit initiation, stabilization, and size. Mol. Biol. Cell *22*, 2588–2600.

Böcking, T., Aguet, F., Harrison, S.C., and Kirchhausen, T. (2011). Single-molecule analysis of a molecular disassemblase reveals the mechanism of Hsc70-driven clathrin uncoating. Nat. Struct. Mol. Biol. *18*, 295–301.

Boucrot, E., Saffarian, S., Massol, R., Kirchhausen, T., and Ehrlich, M. (2006). Role of lipids and actin in the formation of clathrin-coated pits. Exp. Cell Res. *312*, 4036–4048.

Boucrot, E., Saffarian, S., Zhang, R., and Kirchhausen, T. (2010). Roles of AP-2 in clathrin-mediated endocytosis. PLoS ONE *5*, e10597.

Boulant, S., Kural, C., Zeeh, J.C., Ubelmann, F., and Kirchhausen, T. (2011). Actin dynamics counteract membrane tension during clathrin-mediated endocytosis. Nat. Cell Biol. *13*, 1124–1131.

Cureton, D.K., Harbison, C.E., Cocucci, E., Parrish, C.R., and Kirchhausen, T. (2012). Limited transferrin receptor clustering allows rapid diffusion of canine parvovirus into clathrin endocytic structures. J. Virol. *86*, 5330–5340.

Ehrlich, M., Boll, W., Van Oijen, A., Hariharan, R., Chandran, K., Nibert, M.L., and Kirchhausen, T. (2004). Endocytosis by random initiation and stabilization of clathrin-coated pits. Cell *118*, 591–605.

Ferguson, S.M., Raimondi, A., Paradise, S., Shen, H., Mesaki, K., Ferguson, A., Destaing, O., Ko, G., Takasaki, J., Cremona, O., et al. (2009). Coordinated actions of actin and BAR proteins upstream of dynamin at endocytic clathrin-coated pits. Dev. Cell *17*, 811–822.

Fotin, A., Cheng, Y., Sliz, P., Grigorieff, N., Harrison, S.C., Kirchhausen, T., and Walz, T. (2004). Molecular model for a complete clathrin lattice from electron cryomicroscopy. Nature *432*, 573–579.

Gaidarov, I., Santini, F., Warren, R.A., and Keen, J.H. (1999). Spatial control of coated-pit dynamics in living cells. Nat. Cell Biol. *1*, 1–7.

Goodman, O.B., Jr., Krupnick, J.G., Santini, F., Gurevich, V.V., Penn, R.B., Gagnon, A.W., Keen, J.H., and Benovic, J.L. (1996). Beta-arrestin acts as a clathrin adaptor in endocytosis of the beta2-adrenergic receptor. Nature *383*, 447–450.

Gottfried, I., Ehrlich, M., and Ashery, U. (2009). HIP1 exhibits an early recruitment and a late stage function in the maturation of coated pits. Cell. Mol. Life Sci. *66*, 2897–2911.

Harrison, S.C., and Kirchhausen, T. (2010). Structural biology: Conservation in vesicle coats. Nature *466*, 1048–1049.

Henne, W.M., Boucrot, E., Meinecke, M., Evergren, E., Vallis, Y., Mittal, R., and McMahon, H.T. (2010). FCHo proteins are nucleators of clathrin-mediated endocytosis. Science *328*, 1281–1284.

Hinrichsen, L., Meyerholz, A., Groos, S., and Ungewickell, E.J. (2006). Bending a membrane: how clathrin affects budding. Proc. Natl. Acad. Sci. USA *103*, 8715–8720.

Howarth, M., and Ting, A.Y. (2008). Imaging proteins in live mammalian cells with biotin ligase and monovalent streptavidin. Nat. Protoc. *3*, 534–545.

Howarth, M., Liu, W., Puthenveetil, S., Zheng, Y., Marshall, L.F., Schmidt, M.M., Wittrup, K.D., Bawendi, M.G., and Ting, A.Y. (2008). Monovalent, reduced-size quantum dots for imaging receptors on living cells. Nat. Methods *5*, 397–399.

Jaqaman, K., and Danuser, G. (2006). Linking data to models: data regression. Nat. Rev. Mol. Cell Biol. *7*, 813–819.

Jaqaman, K., Loerke, D., Mettlen, M., Kuwata, H., Grinstein, S., Schmid, S.L., and Danuser, G. (2008). Robust single-particle tracking in live-cell time-lapse sequences. Nat. Methods *5*, 695–702.

Kirchhausen, T. (2009). Imaging endocytic clathrin structures in living cells. Trends Cell Biol. *19*, 596–605.

Lee, D.W., Wu, X., Eisenberg, E., and Greene, L.E. (2006). Recruitment dynamics of GAK and auxilin to clathrin-coated pits during endocytosis. J. Cell Sci. *119*, 3502–3512.

Loerke, D., Mettlen, M., Yarar, D., Jaqaman, K., Jaqaman, H., Danuser, G., and Schmid, S.L. (2009). Cargo and dynamin regulate clathrin-coated pit maturation. PLoS Biol. *7*, e57.

Loerke, D., Mettlen, M., Schmid, S.L., and Danuser, G. (2011). Measuring the hierarchy of molecular events during clathrin-mediated endocytosis. Traffic *12*, 815–825.

Massol, R.H., Boll, W., Griffin, A.M., and Kirchhausen, T. (2006). A burst of auxilin recruitment determines the onset of clathrin-coated vesicle uncoating. Proc. Natl. Acad. Sci. USA *103*, 10265–10270.

McMahon, H.T., and Boucrot, E. (2011). Molecular mechanism and physiological functions of clathrin-mediated endocytosis. Nat. Rev. Mol. Cell Biol. *12*, 517–533.

Merrifield, C.J., Feldman, M.E., Wan, L., and Almers, W. (2002). Imaging actin and dynamin recruitment during invagination of single clathrin-coated pits. Nat. Cell Biol. *4*, 691–698.

Mettlen, M., Loerke, D., Yarar, D., Danuser, G., and Schmid, S.L. (2010). Cargo- and adaptor-specific mechanisms regulate clathrin-mediated endocytosis. J. Cell Biol. *188*, 919–933.

Miller, S.E., Sahlender, D.A., Graham, S.C., Höning, S., Robinson, M.S., Peden, A.A., and Owen, D.J. (2011). The molecular basis for the endocytosis of small R-SNAREs by the clathrin adaptor CALM. Cell *147*, 1118–1131.

Nunez, D., Antonescu, C., Mettlen, M., Liu, A., Schmid, S.L., Loerke, D., and Danuser, G. (2011). Hotspots organize clathrin-mediated endocytosis by efficient recruitment and retention of nucleating resources. Traffic *12*, 1868–1878.

Rapoport, I., Miyazaki, M., Boll, W., Duckworth, B., Cantley, L.C., Shoelson, S., and Kirchhausen, T. (1997). Regulatory interactions in the recognition of endocytic sorting signals by AP-2 complexes. EMBO J. *16*, 2240–2250.

Reider, A., Barker, S.L., Mishra, S.K., Im, Y.J., Maldonado-Báez, L., Hurley, J.H., Traub, L.M., and Wendland, B. (2009). Syp1 is a conserved endocytic adaptor that contains domains involved in cargo selection and membrane tubulation. EMBO J. *28*, 3103–3116.

Saffarian, S., Cocucci, E., and Kirchhausen, T. (2009). Distinct dynamics of endocytic clathrin-coated pits and coated plaques. PLoS Biol. *7*, e1000191.

Schwarz, G. (1978). Estimating the dimension of a model. Ann. Stat. *6*, 461–464.

Smith, D.A. (1998). A quantitative method for the detection of edges in noisy time-series. Philos. Trans. R. Soc. Lond. B Biol. Sci. *353*, 1969–1981.

Taylor, M.J., Perrais, D., and Merrifield, C.J. (2011). A high precision survey of the molecular dynamics of mammalian clathrin-mediated endocytosis. PLoS Biol. *9*, e1000604.

Tebar, F., Sorkina, T., Sorkin, A., Ericsson, M., and Kirchhausen, T. (1996). Eps15 is a component of clathrin-coated pits and vesicles and is located at the rim of coated pits. J. Biol. Chem. *271*, 28727–28730.

Toshima, J.Y., Toshima, J., Kaksonen, M., Martin, A.C., King, D.S., and Drubin, D.G. (2006). Spatial dynamics of receptor-mediated endocytic trafficking in budding yeast revealed by using fluorescent alpha-factor derivatives. Proc. Natl. Acad. Sci. USA *103*, 5793–5798.

Traub, L.M. (2009). Clathrin couture: fashioning distinctive membrane coats at the cell surface. PLoS Biol. *7*, e1000192.

von Kleist, L., Stahlschmidt, W., Bulut, H., Gromova, K., Puchkov, D., Robertson, M.J., MacGregor, K.A., Tomilin, N., Pechstein, A., Chau, N., et al. (2011). Role of the clathrin terminal domain in regulating coated pit dynamics revealed by small molecule inhibition. Cell *146*, 471–484.

Yu, A., Rual, J.F., Tamai, K., Harada, Y., Vidal, M., He, X., and Kirchhausen, T. (2007). Association of Dishevelled with the clathrin AP-2 adaptor is required for Frizzled endocytosis and planar cell polarity signaling. Dev. Cell *12*, 129–141.

Zoncu, R., Perera, R.M., Sebastian, R., Nakatsu, F., Chen, H., Balla, T., Ayala, G., Toomre, D., and De Camilli, P.V. (2007). Loss of endocytic clathrin-coated pits upon acute depletion of phosphatidylinositol 4,5-bisphosphate. Proc. Natl. Acad. Sci. USA *104*, 3793–3798.